Journal of Medical Imaging

MedicalImaging.SPIEDigitalLibrary.org

Phase-contrast imaging with a compact x-ray light source: system design

Yongjin Sung
Rajiv Gupta
Brandon Nelson
Shuai Leng
Cynthia H. McCollough
William S. Graves

SPIE.

Yongjin Sung, Rajiv Gupta, Brandon Nelson, Shuai Leng, Cynthia H. McCollough, William S. Graves, "Phase-contrast imaging with a compact x-ray light source: system design," *J. Med. Imag.* **4**(4), 043503 (2017), doi: 10.1117/1.JMI.4.4.043503.

Phase-contrast imaging with a compact x-ray light source: system design

Yongjin Sung,[a] Rajiv Gupta,[b] Brandon Nelson,[c] Shuai Leng,[c] Cynthia H. McCollough,[c,*,†] and William S. Graves[d,†]
[a]University of Wisconsin-Milwaukee, College of Engineering and Applied Science, Milwaukee, Wisconsin, United States
[b]Massachusetts General Hospital, Department of Radiology, Boston, Massachusetts, United States
[c]Mayo Clinic, Department of Radiology, Rochester, Minnesota, United States
[d]Arizona State University, Department of Physics, Tempe, Arizona, United States

Abstract. X-ray phase-contrast imaging (XPCI) overcomes the problem of low contrast between different soft tissues achieved in conventional x-ray imaging by introducing x-ray phase as an additional contrast mechanism. This work describes a compact x-ray light source (CXLS) and compares, via simulations, the high quality XPCI results that can be produced from this source to those produced using a microfocus x-ray source. The simulation framework is first validated using an image acquired with a microfocus-source, propagation-based XPCI (PB-XPCI) system. The phase contrast for a water sphere simulating a simple cyst submersed in muscle is evaluated and the evolution of PB-XPCI signal as the object to detector distance is increased is demonstrated. The proposed design of a PB-XPCI system using the CXLS is described and simulated images of a coronary artery compared between CXLS and microfocus source PB-XPCI systems. To generate images with similar noise levels, a microfocus source would require a 3000 times longer exposure than would the CXLS. We conclude that CXLS technology has the potential to provide high-quality XPCI in a medical environment using extremely short exposure times relative to microfocus source approaches. [DOI: 10.1117/1.JMI.4.4.043503]

Keywords: phase-contrast CT; compact x-ray light source; microfocus x-ray sources.

Paper 17236R received Aug. 2, 2017; accepted for publication Nov. 6, 2017; published online Nov. 23, 2017.

1 Introduction

X-ray computed tomography (CT) is used in preclinical and clinical imaging to determine the x-ray attenuation properties of materials in three-dimensions (3-D). Specifically, CT measures the x-ray linear attenuation coefficient, which is related to the imaginary portion ($\boldsymbol{\beta}$) of the complex refractive index n, where $n = 1 - \boldsymbol{\delta} - i\boldsymbol{\beta}$. The real portion ($\boldsymbol{\delta}$) characterizes the phase shifting properties of a material. Of particular importance is the fact that $\boldsymbol{\delta}$ is approximately three orders of magnitude larger than $\boldsymbol{\beta}$. After converting the phase information into measurable signal, this can result in a significant increase in contrast and an opportunity for reduced dose requirements. For different types of soft tissues, the linear attenuation coefficient obtained by conventional CT is unable to discriminate between materials of similar composition.[1] X-ray phase-contrast imaging (XPCI) overcomes this fundamental limitation of conventional x-ray imaging—the lack of contrast between different soft tissues—by introducing x-ray phase as an additional contrast mechanism. XPCI thus augments the ability to nondestructively characterize soft tissue pathology, paving the way for new preclinical and clinical applications.

In XPCI, refractive index differences among tissue types manifest as small angular deviations ($\sim 10^{-4}$ to 10^{-5} deg) in the x-ray beampath. Capturing these small angular deviations as contrast in an acquired x-ray image requires a spatially coherent x-ray source. More generally, the ability to make use of phase contrast depends on the properties of the x-ray beam, the optics used to manipulate the beam, and the capabilities of the detector that records the image. A variety of successful experimental XPCI setups have been reported.[2–12] However, despite its promise, to date there are no XPCI systems in clinical use. A key factor contributing to this lack of clinical adoption is the unavailability of a compact x-ray source suitable for a hospital environment that has the coherence and beam properties required for XPCI.

The x-ray beam properties that are important for XPCI include its apparent focal spot size, divergence, photon energy, energy bandwidth, and flux. The type of source used to produce an x-ray beam largely determines these properties. Traditional rotating anode x-ray tubes are widely used for clinical imaging due to their convenient size, reliability, and relatively low cost. However, these x-ray sources produce an incoherent x-ray beam with a modest photon flux that is unsuitable for some phase-contrast imaging techniques. Several other properties—e.g., large focal spot size, large beam divergence, wide energy bandwidth, and inability for submillisecond exposure times—also make them a poor source for XPCI. Microfocus x-ray sources focus electron beams to a very small spot on the target, with a size on the order of 10 μm. The x-rays generated from such a small focal spot have a relatively high spatial coherence, which is important in XPCI. However, microfocus sources can produce only very low photon flux and are hence not applicable to clinical imaging.

*Address all correspondence to: Cynthia H. McCollough, E-mail: mccollough.cynthia@mayo.edu

†Drs. McCollough and Graves are both senior authors for this work.

2329-4302/2017/$25.00 © 2017 SPIE

Traditionally, synchrotron radiation sources have been used to provide the high output, coherent, monoenergetic x-rays required for XPCI, and multiple different paradigms for XPCI have been demonstrated using the powerful x-ray beams available at large synchrotron facilities.[2–4,13] Synchrotron-based x-ray sources produce x-ray beams that are more than a billion times brighter than rotating anode x-ray tubes. Because a large photon flux is available, one can use specialized optics to subselect from the available flux a narrow band of coherent x-ray photons that will contribute to the phase image generation. Even though a majority of the x-ray beam is wasted by the x-ray optics, excellent XPCI performance has been demonstrated using synchrotron beamlines. Nevertheless, the size, complexity, and infrastructure cost of a synchrotron effectively preclude its use for routine clinical imaging.

In this paper, we describe a new x-ray source that is based on inverse Compton scattering (ICS),[14] which we refer to as a compact x-ray light source (CXLS). This x-ray source has performance characteristics that are intermediate between a large synchrotron and a rotating anode x-ray tube. Similar to a large synchrotron, an ICS source uses a small accelerator to produce relativistic electrons. However, unlike a synchrotron, which uses magnetic wigglers or undulators, an ICS source uses a laser whose electromagnetic field wiggles the electrons to produce bursts of x-rays. The much shorter period of the laser allows the electrons to produce hard x-rays at lower electron energy than a synchrotron, resulting in a compact device that is only a few meters long. The resulting x-ray beam shares many similarities with a synchrotron x-ray beam, including high average flux, narrow cone of divergence, monochromatic bandwidth of a few percent, tunable photon energy, and polarized output. The x-ray output is temporally modulated and arrives in short picosecond pulses. The source focal spot size, which is important for XPCI, can be less than 10 μm, roughly an order of magnitude smaller than a typical focal spot from a rotating anode tube used for radiography or x-ray CT. A CXLS built using the ICS principle provides an attractive source for XPCI because it offers high photon flux with coherent and tunable x-rays from a compact assembly that can be sited in a hospital environment.

In this paper, we summarize the key features and performance metrics of the CXLS currently being built at Arizona State University.[15] We also describe how the x-ray beam from CXLS can be applied to XPCI imaging. A detailed simulation framework is introduced that models the CXLS and simulates the phase images that can be expected from a propagation-based XPCI (PB-XPCI) system built using the described CXLS. Finally, we present results from this detailed simulation to illustrate the quality of XPCI that will be enabled by CXLS.

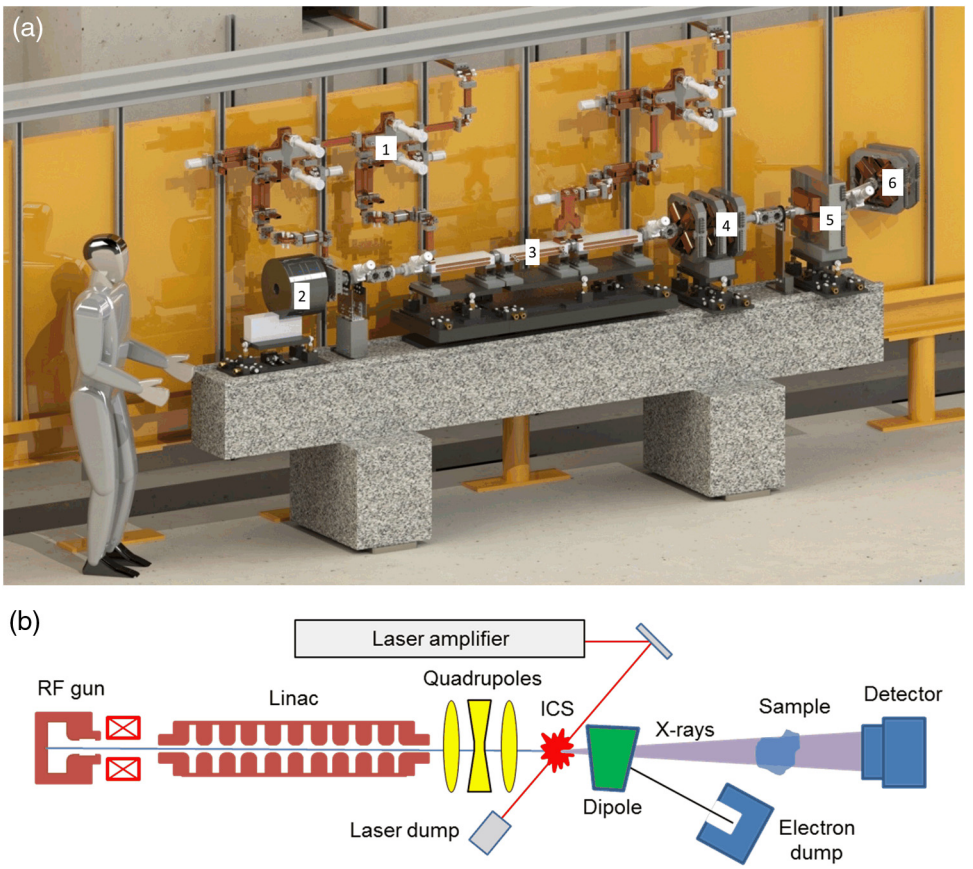

Fig. 1 (a) CAD model of CXLS accelerator where (1) is RF waveguide, (2) is solenoid magnet enclosing photoinjector that produces the electron beam, (3) is the short linear accelerator, (4) are quadrupole magnets to focus the electron beam to a small spot, (5) is a dipole magnet, and (6) are quadrupole magnets leading to the electron beam dump. (b) Schematic of CXLS components including laser, sample, and detector. The laser is housed in an adjacent clean room and the sample area and x-ray detector are in a hutch to the right of accelerator in upper figure.

2 Methods

2.1 *X-Ray Production Via Inverse Compton Scattering*

X-rays are emitted by ICS when a relativistic electron beam collides with a laser pulse in a nearly head-on geometry (i.e., 50 mrad) (Fig. 1). ICS sources are a fraction of the size of a synchrotron because the electron energy needed to produce hard x-rays via ICS is much lower than for a synchrotron. Both sources rely on electrons wiggling in a sinusoidally varying electromagnetic field, but with a dramatic difference in the length of the undulator period. A static undulator used for synchrotron x-ray production has a period of several centimeters, or more than ten thousand times longer than the laser wavelength used for ICS. The electron energy required to make a particular x-ray photon energy scales as the square root of the period of the field used to wiggle the electrons. As a result, an ICS accelerator is more than one hundred times smaller than a traditional synchrotron source, fitting comfortably into existing medical facilities. The lower electron energy can be produced by a small linear accelerator (linac)[15] or a small synchrotron.[16] Synchrotron-based approaches enable higher repetition rates than linacs; however, the beam properties of synchrotrons (relatively long pulses with poor emittance) result in larger source sizes with many fewer photons per shot and lower overall flux and brilliance than a linac-based source. Synchrotrons also require a linac for injection of the electron beam, hence are larger, more complicated, and expensive devices than just a linac alone. The linac-based approach, which we adopt, avoids these drawbacks.

The x-ray wavelength, or photon energy, produced is determined by the electron beam energy and the laser wavelength. Photon energy can be tuned over a wide range on a timescale of seconds by changing the electron beam energy in the linac. The maximum linac energy in our current configuration is $E = 35$ MeV, yielding a maximum photon energy of 45 keV. These x-rays are monochromatic, in contrast to the polychromatic bremsstrahlung x-rays produced by a conventional x-ray tube.

The source size of the x-ray beam is approximately the same as the electron beam size, which has a 10 μm diameter at the moment of collision. It is this very small source size, combined with the monochromatic output, which provides the coherence necessary for optimum phase-contrast imaging. Complete details regarding the CXLS can be found in Ref. 15; a summary of the relevant parameters used in the CXLS simulation is presented in Table 1.

Table 1 X-ray parameters for the described CXLS.

Parameter	Value	Units
Monochromatic x-ray energy	<45	keV
Time averaged flux	1×10^{15}	photons/s/sr
Source diameter	10	μm
Source divergence	8	mrad
Photons per pulse	5×10^{7}	photons per shot
Pulse length	1	picosecond
Repetition rate	1000	Hz

2.2 *Phase-Contrast Imaging Systems*

As mentioned previously, in conventional x-ray imaging, image contrast arises from the attenuation of x-rays due to photoelectric absorption and Compton scattering, with attenuation contrast being sensitive to the difference in atomic number and electron density. As a result, bone pathology is generally well seen in x-ray radiography while soft tissue abnormalities may be hard to detect. XPCI explores an alternative mechanism of interaction between the x-ray wave and tissue, namely phase alteration or bending of x-rays due to electron clouds of various materials. This allows XPCI to improve soft tissue contrast compared to attenuation-based x-ray imaging.[17] For example, we have shown that XPCI can characterize atherosclerotic plaque and discriminate benign from cancerous tissue.[13]

A variety of XPCI systems have been demonstrated using both synchrotrons[2–4,7,12] as well as laboratory-scale x-ray sources.[6,10,11,18,19] All these systems, so far, are only suitable for small *ex vivo* specimens and small animals. Considerable efforts are being made to scale up the size of these phase-contrast imaging systems for human imaging.[20,21] A key technical limitation in this area, something that CXLS can remedy, is the lack of a coherent source that can be deployed in a hospital setting. Table 2 lists the various methods used for XPCI, along with their major advantages and disadvantages. Table 3 compares the suitability of various x-ray sources for XPCI.

2.3 *Simulation of X-Ray Phase-Contrast Imaging*

In XPCI, the phase alteration of x-rays induced by a sample serves as imaging contrast. The phase alteration can be best predicted using wave optics, whereas geometrical optics or ray tracing suffices to calculate the attenuation in conventional x-ray imaging.

XPCI simulation consists of two steps: (i) modeling the interaction of x-rays with the 3-D structure of the sample, during which the phase of the incident x-ray beam is altered, and (ii) modeling the conversion of the phase, which cannot be directly recorded, to the x-ray amplitude that can be recorded using a conventional x-ray detector.

In XPCI, the interaction of x-rays with the 3-D structure of sample can be calculated by solving the wave equation. The computational cost for directly solving the wave equation, however, is prohibitively large for the size of the objects typically used in XPCI. In early pioneering studies, the projection approximation was used, ignoring the wave nature of x-rays within the sample but including it only in the free-space propagation. In other studies, ray tracing or geometrical optics was used, including refraction or bending of x-rays within the sample. In our recent work, we used the first-order Rytov approximation, which is accurate in XPCI, to simplify the wave equation. We applied this model to the x-ray-object interaction as well as to the free-space propagation.[22] Our full-wave approach can be used for simulating XPCI using an x-ray source with a finite focal spot and a broadband energy spectrum.

As with other imaging simulations, XPCI simulation requires a 3-D phantom as an input. For realistic simulation of conventional x-ray imaging, a voxelated phantom is typically used. For absorption-based simulation, a discretized phantom does not

Table 2 Methods used for XPCI.

Method	Advantages	Disadvantages
Crystal interferometry	• High sensitivity to changes in electron density • High sensitivity to low spatial frequency features	• Requires exceptional mechanical stability • Limited field of view in the hard x-ray regime • Requires monochromatic and highly collimated beam
Analyzer-based imaging	• Less requirements on the mechanical stability than crystal interferometry	• Requires monochromatic and highly collimated beam • Limited field of view due to the needs of a flat and pure analyzer crystal and a parallel beam geometry • Less sensitive to low spatial frequencies features
Propagation-based imaging	• Least complicated setup in terms of optics and mechanical assemblies • Fast if using single-distance acquisition and retrieval algorithm (or even two-distance for more quantitative information) • High sensitivity to the interface of material phases with distinct complex index of refraction in the specimen • Can work with synchrotron radiation sources and also x-ray tube sources (cone beam, polychromatic spectrum)	• Loss of quantitative information if using single distance acquisition method • Complexity of holography phase retrieval • High requirement on the coherence of x-ray source and small detector pixel size • Long propagation distance from sample-to-detector when working with partial coherent source and moderate detector pixel size
Grating-based imaging	• Additional dark-field contrast imaging with high sensitivity to the microscopic local electron density fluctuation below spatial resolution of imaging system, by exploiting the ultrasmall angle scattering of x-ray • Able to be implemented with synchrotron radiation and x-ray tube • Provides independent phase and absorption images, providing quantitative imaging properties	• Expense of grating fabrication, especially for higher x-ray energy • Field of view limited by size of G2 (detector) grating

degrade the quality of the simulated image as long as the voxel size is properly selected in relation to the detector pixel size. Improper matching of voxel size to pixel size can result in noticeable artifacts.[23] This effect is amplified when applied to XPCI simulation, where the discretized phantom creates phase signal artifacts at the voxel boundaries that cannot be distinguished from those generated from small features in a real object. Decreasing the phantom voxel size can reduce this effect but quickly increases the computation time, which is inversely proportional to the voxel volume. To overcome this limitation, we have incorporated into our full-wave model the four-dimensional extended cardiac-torso (XCAT) phantom, which is represented with nonuniform rational B-splines (NURBS).[24] The continuous (i.e., nonvoxelized) NURBS-based full-wave model allows us to simulate XPCI with high accuracy without the artifact caused by the discretized phantom. For the complex refractive index value, we used the data in "Photon, Electron, Proton, and Neutron Interaction Data for Body Tissues" from the International Commission on Radiation Units and Measurements.[1]

Table 3 Comparison of x-ray sources for XPCI. The specific requirement for each parameter depends on the type and design of the XPCI system.

	Coherence			
	Focal spot size (spatial coherence)	Spectral bandwidth (temporal coherence)	Brilliance	Field of view size
Rotating-anode x-ray tube	Poor	Poor	Good	Good
Synchrotron	Good	Good	Good	Poor
Microfocus source	Good	Poor	Poor	Good
CXLS	Good	Good	Good	Good

Because of the small focal spot size (10 μm) of the CXLS, we may assume that the x-ray beam incident on the imaged specimen is a plane wave, which helps reduce the computation time compared to using a model for a partially coherent x-ray source with spherical waves. The geometric magnification due to the cone-beam geometry is included in the simulation model. The phase-contrast signal is usually smoothened due to a broad energy spectrum. However, the energy bandwidth of CXLS is expected to be less than 5% of the mean energy. Therefore, in the simulations, we assumed monoenergetic x-rays for CXLS,

whereas we included the full energy spectrum for a microfocus source. The energy spectrum of the microfocus source was obtained from a simulator[25] of a tungsten anode at a peak voltage 40 kVp with a 200-μm beryllium window. This is typical of microfocus tubes such as the tube used for experimental data collection. For the CXLS, because of the narrow energy bandwidth, beam filter is not required.

Using a single graphics card (NVIDIA, Tesla K40C) capable of general-purpose computing on graphics processing units, the computation took about 3.3 days to generate a 2048×2048 XPCI image from an NURBS phantom with 8.8 million control points. Further details of the simulation method can be found in our recent publication.[26]

2.4 *Simulation Validation*

The simulation framework used in this study was validated with the exact Mie solution.[27] For further validation, we acquired an image of a bead using a PB-XPCI system and compared it with the simulation. Figure 2(a) shows the imaging geometry. The source-to-sample distance was 0.2 m and the sample-to-detector distance was 1.85 m. The sample was a polyethylene bead (Cospheric LLC) with a diameter of 600 μm. A microfocus source (Hamamatsu Corp., L8121-03) was used at a tube voltage of 40 kVp, a tube current of 100 μA, and an exposure time of 400 s. A custom built x-ray detector from Radiation Monitoring Devices, Inc. with a pixel size of 16 μm was used in the simulation and experimental system. To extract a representative one-dimensional (1-D) profile across the center of the bead in the raw image [Fig. 2(c)], we averaged the pixel intensities along the circumference of the bead. For the simulation, we assumed an x-ray source with a photon flux of 3.2×10^{11} photons/s/sr, which approximated the noise in the background region [rectangle in Fig. 2(d)] at the same level (1.2% of the mean intensity value) as in the experimentally acquired image [rectangle in Fig. 2(c)]. The mass attenuation coefficient of polyethylene at different energies was derived from the NIST website[28] but a large variation in the value is expected depending on the exact composition of the material. Therefore, in the simulation, we adjusted the mass attenuation coefficient and the electron density of the sample to match the amplitude of the 1-D profile with the experimental data and then tested the profile agreement.

2.5 *Design of a PB-XPCI System Using CXLS*

For the CXLS to be built in this project, we are designing an imaging chain for PB-XPCI with a source-to-sample distance of 3.5 m and a sample-to-detector distance of 4.5 m. Using a 4096×4112 detector with pixel size of 15 μm, such as the Andor iKon-XL (Andor Technology Ltd., Belfast, Northern Ireland) we expect to get an image of an object as big as 22.4×22.4 mm^2 using a lens with unity magnification. Larger objects

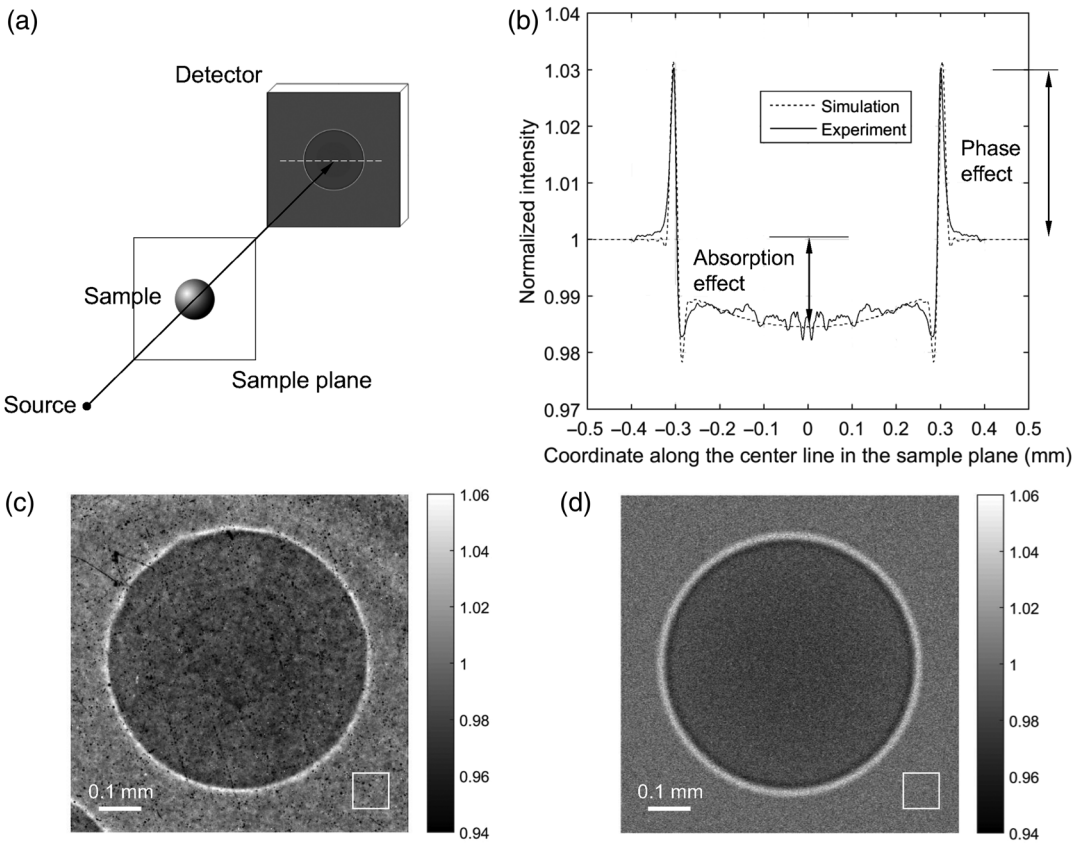

Fig. 2 Validation of the simulation framework used in this study: (a) cone-beam propagation-based x-ray phase-contrast imaging geometry; (b) comparison of the simulated cross section profile with the experimental data; (c) experimentally acquired image of a polyethylene bead; and (d) simulated bead image. The noise texture differs between (c) and (d) due to detector effects that were not modeled in the simulation, such as imperfections in the physical detector.

may be imaged by using lenses with magnification less than unity.

In PB-XPCI, the phase-contrast signal is proportional to the Laplacian of the projected electron density; thus, it is manifested as bright and dark rings around the edge of an object. To quantitatively predict this contrast enhancement, we simulated the XPCI image of a sphere with varying x-ray energies ranging from 10 to 35 keV and for sphere diameters of 0.5 to 5 mm. For each simulated image, we calculated the difference between signal and background and normalized the difference by the background; this was defined as the phase contrast.

2.6 *Comparison of XPCI Using CXLS and a Microfocus X-Ray Tube*

For this simulation, we extracted from the XCAT phantom,[23] the NURBS models that represented the right coronary artery, and one of its acute marginal branches. These coronary arteries were virtually embedded in a 3-cm-thick myocardial tissue simulant. We assigned the complex refractive index for water to the arteries and the value for muscle to the surrounding tissue and applied a median filter of size 3×3. The region inside the artery was assumed to be composed of muscle and outside the artery was assumed to be water.

3 Results

3.1 *Validation of Simulation Framework: Comparison with Experimental Data*

Figure 2 shows the comparison of simulation and experimental data. The accurate match between the 1-D profiles [Fig. 2(b)], together with the similarity between Figs. 2(c) and 2(d), confirms the validity of our simulation framework.

3.2 *Design of a PB-XPCI System Using CXLS*

XPCI converts the sample-induced x-ray phase delay into an amplitude that can be recorded using a conventional x-ray detector. In PB-XPCI, this conversion occurs as the beam propagates in free-space; thus, the phase-contrast signal becomes stronger with increasing propagation distance. Figure 3 shows this enhancement of phase contrast as the sample-to-detector distance increases from 3 to 10 m. The source energy was fixed at 26 keV for this calculation. All the other parameters were fixed at the same values as used in the previous simulation. For a diameter of 1 mm, the phase contrast increased by 2.8 times from 0.036 to 0.099, when the sample-to-detector distance increased from 4.5 to 10 m. For a larger bead, the phase contrast increased by a similar amount. For example, for a diameter of 5 mm, the phase contrast increased by 2.9 times from 0.084 to 0.24, when the sample-to-detector distance increased from 4.5 to 10 m.

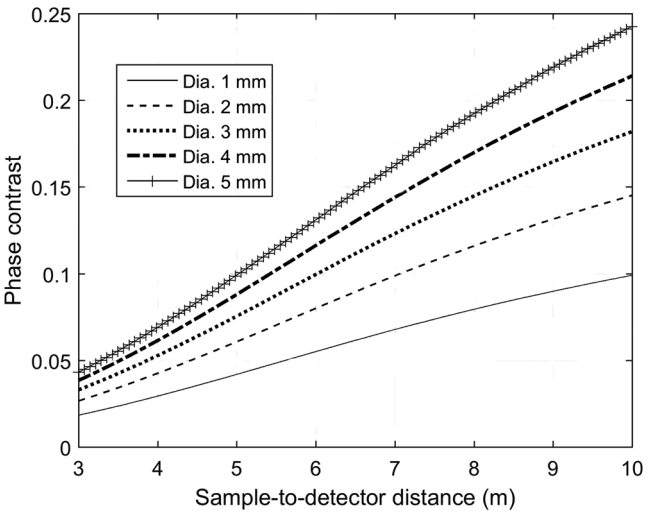

Fig. 3 Contrast enhancement for different sample-to-detector distances due to the tradeoff between photon flux and the evolution of PB-XPCI signal, as well as the enhancement due to magnification.

Of note, the increased phase contrast comes at the cost of reduced photon flux due to the larger source-to-detector distance, and thus increased Poisson noise if exposure time was kept the same. We expect CXLS to generate about 10^{15} photons/s/sr. For the system design described here (i.e., sample-to-detector distance 4.5 m), the photon flux onto each detector pixel is about 3×10^3 photons/s/pixel, when there is 70% attenuation of x-rays by a sample (e.g., a 3-cm-thick tissue specimen). The Poisson noise due to this random arrival of x-ray photons is about 1.8% of the mean intensity. When the sample-to-detector distance increases to 10 m, the photon flux decreases to about 10^3 photons/s/pixel and the Poisson noise increases to 3.1%, which is about 1.7 times higher than the previous Poisson noise. This increase in Poisson noise, together with the increased system footprint, should be considered when increasing the sample-to-detector distance for enhanced phase contrast.

3.3 *Comparison of XPCI Using CXLS and a Microfocus X-Ray Tube*

Figures 4(a)–4(c) compare the simulated XPCI images that CXLS will generate for different exposure times: 1, 3, and 10 s. Figure 4(d) shows the simulated XPCI image that a conventional microfocus x-ray source will generate for the exposure time of 10 s. In Figs. 4(a) and 4(b), the arteries can be identified, although the inset figures show that the noise is as strong as the phase-contrast signal. The region inside the artery is slightly brighter than the background because the linear attenuation coefficient of muscle is greater than that of water. Due to the differential phase contrast between the artery and water, the boundary of the artery looks darker, which helps to identify it. The inset graph in each figure is the cross sectional profile along the dotted line. The diameters of the arteries are 1.7 and 1.1 mm at the intersections with the dotted line. When the exposure time increases to 10 s, the phase-contrast signals at the edges can be clearly distinguished from the fluctuating background noise. Of note, the XPCI image that a microfocus source would generate for the same exposure time of 10 s [Fig. 4(d)] does not show the arteries because of the high noise level 39%. A microfocus tube XPCI image of similar noise characteristics to Fig. 4(c) would require >30,000 s to acquire.

4 Discussion

Several teams around the world have been exploring preclinical, and to a lesser extent, clinical applications of XPCI for decades. This is particularly true for applications such as breast imaging, where soft tissue contrast is of paramount importance. These endeavors hope to take advantage of the enhanced soft tissue contrast characteristic of XPCI in order to improve sensitivity and specificity. For example, screening mammography has

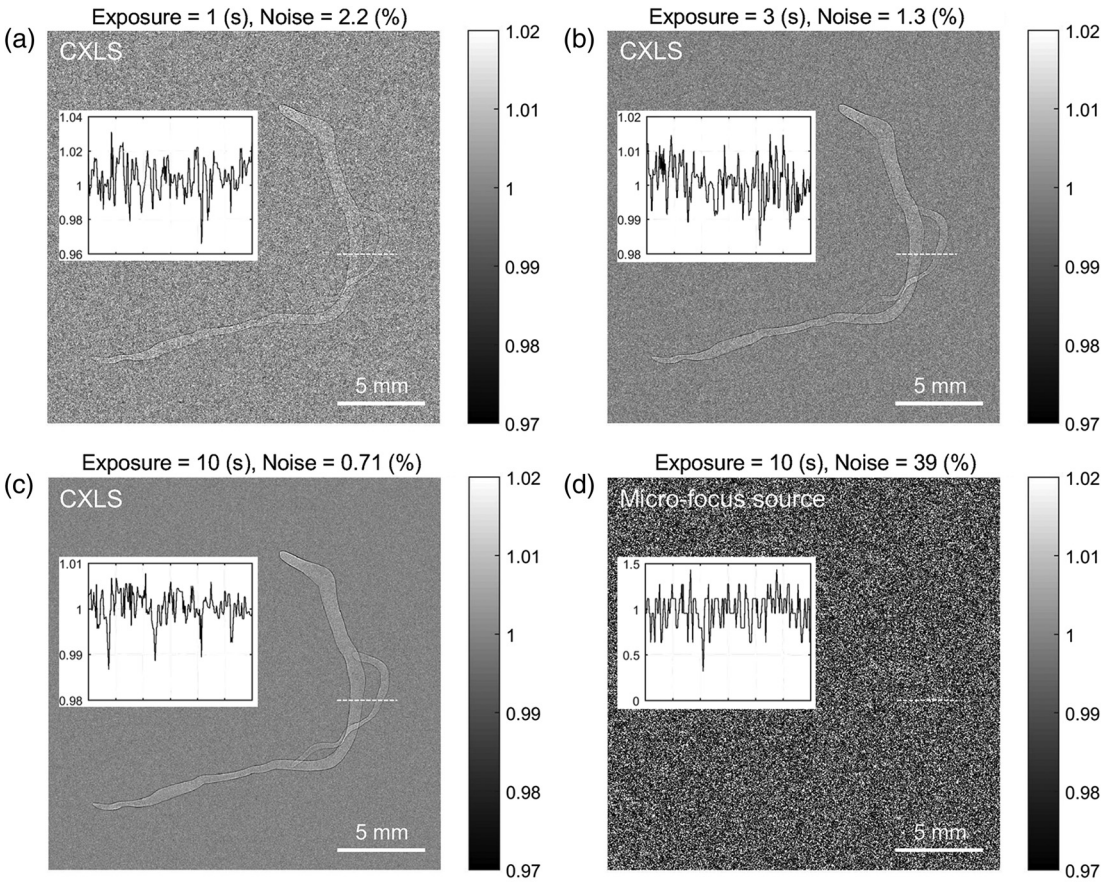

Fig. 4 Simulation of PB-XPCI using the design parameters for the system under construction. The sample is the right coronary artery included in the XCAT digital phantom. (a), (b), and (c) were simulated with CXLS, and (d) with a microfocus x-ray tube source.

increased detection of ductal carcinoma *in situ*, an early stage cancer; however, current screening mammography suffers from poor sensitivity and specificity due to limited soft tissue contrast,[29] resulting in high false-positive and false-negative rates that limit its effectiveness and demonstrate the need for improved screening methods.[30,31] Initial studies into phase-contrast planar mammography using *ex vivo* specimens suggest better visualization of the fine structural detail of the breast, revealing fine collagen strands and better delineation of boundaries between glandular and adipose tissue.[32] Others have focused on optimizing the soft tissue signal from XPCI in the breast with iterative reconstructions and hybrid imaging that combines the edge delineation and small feature resolution characteristics of phase contrast and dark-field imaging with the attenuation signal in a single fused image.[33,34] Thus, advances in XPCI have the potential to greatly increase visibility of small features in mammography and improve its efficacy. Similar arguments could be made for other oncologic and nononcologic imaging applications of XPCI.

Currently, most XPCI techniques require a synchrotron for fast imaging; XPCI systems with laboratory x-ray sources are available; however, imaging times are prohibitively long. A limitation to having synchrotron quality x-rays available for clinical or biomedical use is the large size of accelerators needed to produce x-ray radiation. The application of laser driven, rather than magnetic, undulators has been demonstrated by the compact light source produced by Lyncean Technologies;[35] the Munich Compact Light Source (MuCLS) is currently in operation and is being used for biomedical applications.[35] The MuCLS incorporates both a linac and a small synchrotron ring to accelerate the electrons and maintain their energy. The use of a synchrotron results in a larger and more complex x-ray source, where the electron beam has longer pulses, poorer emittance, and larger source size. These attributes result in a more expensive device that produces an x-ray beam with lower brilliance and flux than that produced by a high brightness linac. The linac-based source can also change photon energy on a subsecond timescale, which is not possible with the synchrotron.

In this paper, we present the specifications and operating characteristics of a linac-based CXLS that generates a bright, monochromatic, coherent x-ray beam using ICS. Linear accelerators are already a clinical workhorse in external beam radiation therapy, with over 10,000 in use worldwide.[36] A linac-based compact light source could expand their clinical use to diagnostic imaging.

Several features of CXLS are attractive for XPCI. The small focal spot size of the CXLS results in minimal geometric blurring and the resultant high spatial coherence preserves the phase information of the object. The high photon flux of CXLS allows image formation to require less than 1/3000 the time required for a microfocus source [Figs. 4(c) and 4(d)]. In XPCI, such short exposure times are crucial for reducing potential motion artifacts or artifacts arising from source or specimen instability. Finally,

the use of a CXLS overcomes the technical hurdles facing several phase-contrast methods by providing a monochromatic and highly collimated x-ray source. These considerations make CXLS an attractive choice for XPCI.

In order to test the imaging characteristics of our CXLS, we constructed a simulation framework using the first-order Rytov approximation and validated our simulation technique by showing agreement between the simulated and experimentally acquired microfocus source images. This simulation framework was then used to compare the CXLS and a microfocus source. Our results showed that phase-contrast images generated from the CXLS offer superior contrast over methods using a traditional microfocus source. In addition, due to the synchrotron-like photon flux from the CXLS, the images can be acquired in a fraction of the exposure time as compared with a microfocus source.

For PB-XPCI, our simulation results demonstrated the potential for image quality improvement using CXLS compared to microfocus x-ray sources. Our results also suggest the benefits of CXLS in conventional absorption contrast applications. A recent study showed that quasimonoenergetic photons from another compact light source improved the contrast-to-noise ratio in coronary angiography via iodine K-edge absorption imaging, allowing for reduction in contrast media while achieving improved image quality.[16] Our findings suggest that XPCI using CXLS could further complement coronary angiography by enhancing vessel delineation and improving soft tissue contrast, as shown in Fig. 4(c). This raises the exciting possibility that high quality phase and attenuation information could be extracted simultaneously in clinical or laboratory setting, without needing a synchrotron facility. The current iteration of the CXLS has a maximum x-ray energy of 45 keV, making it suitable for imaging of the breast, extremities, small animals, and *ex vivo* specimens. However, higher energies will be necessary before imaging of thicker body regions is possible with such a source. Higher photon energies are achieved by simply adding larger power supplies to the device at additional cost. There are no technical barriers to reaching higher energy, and the performance of the source improves at higher energy. Further development of these compact light sources may make these clinical XPCI applications a reality.

5 Conclusion

In the century since their discovery by William Roentgen, x-ray production techniques and the use of attenuation contrast mechanisms have remained largely unchanged. This work has presented the key features of a new generation of compact light sources and demonstrated the high quality phase-contrast images produced from this source via simulations. We conclude that advances in compact light source technology have the potential to revolutionize x-ray imaging, whereby multiple imaging contrast mechanisms (phase and attenuation) can be incorporated into clinical and biomedical laboratories rather than being limited to large synchrotron facilities. These advances may benefit biomedical researchers and patients via improved soft tissue sensitivity complementing existing attenuation contrast mechanisms.

Disclosures

Dr. McCollough receives grant funding from Siemens Healthcare for work unrelated to this project. No other authors report a potential conflict of interest.

Acknowledgments

The project described was supported by a Team Science Award from Mayo Clinic and Arizona State University. The Tesla K40 used for this research was donated by NVIDIA Corporation. Dr. Gupta's research was supported in part by the following contracts: (a) DoD W81XWH-13-2-0067, (b) DoD CDMRP Air Force Contract # FA8650-17-C-9113, (c) USAMRAA W81XWH-15-C-0052, and (d) USAMRAA W81XWH-17-C-0068.

References

1. International Commission on Radiation Units and Measurements, *Photon, Electron, Proton, and Neutron Interaction Data for Body Tissues*, International Commission on Radiation Units and Measurements, Bethesda, Maryland (1992).
2. M. Ando et al., "Simple x-ray dark- and bright-field imaging using achromatic lane optics," *Jpn. J. Appl. Phys.* **41**, L1016–L1018 (2002).
3. U. Bonse and M. Hart, "An x-ray interferometer," *Appl. Phys. Lett.* **6**, 155–156 (1965).
4. D. Chapman et al., "Diffraction enhanced x-ray imaging," *Phys. Med. Biol.* **42**, 2015–2025 (1997).
5. C. David et al., "Differential x-ray phase contrast imaging using a shearing interferometer," *Appl. Phys. Lett.* **81**, 3287–3289 (2002).
6. Y. S. Kashyap et al., "Laboratory-based x-ray phase-contrast imaging technique for material and medical science applications," *Appl. Radiat. Isot.* **66**, 1083–1090 (2008).
7. A. Momose et al., "Demonstration of x-ray Talbot interferometry," *Jpn. J. Appl. Phys.* **42**, L866–L868 (2003).
8. K. S. Morgan, D. M. Paganin, and K. K. W. Siu, "Quantitative single-exposure x-ray phase contrast imaging using a single attenuation grid," *Opt. Express* **19**, 19781–19789 (2011).
9. A. Olivo et al., "An innovative digital imaging set-up allowing a low-dose approach to phase contrast applications in the medical field," *Med. Phys.* **28**, 1610–1619 (2001).
10. F. Pfeiffer et al., "Phase retrieval and differential phase-contrast imaging with low-brilliance x-ray sources," *Nat. Phys.* **2**, 258–261 (2006).
11. H. Wen et al., "Spatial harmonic imaging of x-ray scattering: initial results," *IEEE Trans. Med. Imaging* **27**, 997–1002 (2008).
12. S. W. Wilkins et al., "Phase-contrast imaging using polychromatic hard x-rays," *Nature* **384**, 335–338 (1996).
13. M. Ando et al., "Crystal analyser-based x-ray phase contrast imaging in the dark field: implementation and evaluation using excised tissue specimens," *Eur. Radiol.* **24**, 423–433 (2014).
14. W. J. Brown et al., "Experimental characterization of an ultrafast Thomson scattering x-ray source with three-dimensional time and frequency-domain analysis," *Phys. Rev. Spec. Top. Accel. Beams* **7**(6), 060702 (2004).
15. W. S. Graves et al., "Compact x-ray source based on burst-mode inverse Compton scattering at 100 kHz," *Phys. Rev. Spec. Top. Accel. Beams* **17**(12), 120701 (2014).
16. E. Eggl et al., "Mono-energy coronary angiography with a compact synchrotron source," *Sci. Rep.* **7**, 42211 (2017).
17. D. Paganin, *Coherent X-Ray Optics*, Oxford University Press, Oxford, New York (2006).
18. Y. S. Ge et al., "Grating based x-ray differential phase contrast imaging without mechanical phase stepping," *Opt. Express* **22**, 14246–14252 (2014).
19. W. Zhou, K. Majidi, and J. G. Brankov, "Analyzer-based phase-contrast imaging system using a micro focus x-ray source," *Rev. Sci. Instrum.* **85**, 085114 (2014).
20. J. Keyrilainen et al., "Phase-contrast x-ray imaging of breast," *Acta Radiol.* **51**, 866–884 (2010).
21. A. Tapfer et al., "Experimental results from a preclinical x-ray phase-contrast CT scanner," *Proc. Natl. Acad. Sci. U. S. A.* **109**, 15691–15696 (2012).
22. Y. J. Sung et al., "Full-wave approach for x-ray phase imaging," *Opt. Express* **21**, 17547–17557 (2013).
23. A. L. Goertzen, F. J. Beekman, and S. R. Cherry, "Effect of voxel size in CT simulations," in *IEEE Nuclear Science Symp.* (2000).

24. W. P. Segars et al., "4D XCAT phantom for multimodality imaging research," *Med. Phys.* **37**, 4902–4915 (2010).
25. Siemens, "Simulation of x-ray spectra," 2017, https://www.oem-xray-components.siemens.com/x-ray-spectra-simulation (13 July 2017).
26. Y. J. Sung et al., "Realistic wave-optics simulation of x-ray phase-contrast imaging at a human scale," *Sci. Rep.* **5**, 12011 (2015).
27. Y. J. Sung and G. Barbastathis, "Rytov approximation for x-ray phase imaging," *Opt. Express* **21**, 2674–2682 (2013).
28. J. H. Hubbell and S. M. Seltzer, "Tables of x-ray mass attenuation coefficients and mass energy-absorption coefficients (version 1.4)," 1996, http://physics.nist.gov/xaamdi
29. C. Kuhl et al., "Prospective multicenter cohort study to refine management recommendations for women at elevated familial risk of breast cancer: the EVA trial," *J Clin Oncol.* **28**, 1450–1457 (2010).
30. N. Howlader et al., *SEER Cancer Statistics Review, 1975-2014*, National Cancer Institute, Bethesda, Maryland (2017).
31. O. Olsen and P. C. Gotzsche, "Cochrane review on screening for breast cancer with mammography," *Lancet* **358**, 1340–1342 (2001).
32. J. Keyrilainen et al., "Visualisation of calcifications and thin collagen strands in human breast tumour specimens by the diffraction-enhanced imaging technique: a comparison with conventional mammography and histology," *Eur. J. Radiol.* **53**, 226–237 (2005).
33. K. Bliznakova et al., "A software platform for phase contrast x-ray breast imaging research," *Comput. Biol. Med.* **61**, 62–74 (2015).
34. E. Coello et al., "Fourier domain image fusion for differential x-ray phase-contrast breast imaging," *Eur. J. Radiol.* **89**, 27–32 (2017).
35. E. Eggl et al., "X-ray phase-contrast tomography with a compact laser-driven synchrotron source," *Proc. Natl. Acad. Sci. U. S. A.* **112**, 5567–5572 (2015).
36. U. Amaldi et al., "Accelerators for hadrontherapy: from Lawrence cyclotrons to linacs," *Nucl. Instrum. Methods Phys. Res., Sect. A* **620**, 563–577 (2010).

Yongjin Sung is an assistant professor of mechanical engineering and biomedical engineering at the University of Wisconsin-Milwaukee. His research interests focus on developing imaging techniques including phase-contrast imaging in the visible and the x-ray regimes, 3-D imaging flow cytometry, and radioluminescence microscopy. He received his doctorate from the Massachusetts Institute of Technology in 2011.

Rajiv Gupta is an associate radiologist in the neuro and emergency radiology divisions at Massachusetts General Hospital, an associate professor of radiology at Harvard Medical School, and a lecturer in mechanical engineering at MIT. He earned his MD at Cornell University and his PhD in computer science at the State University of New York at Stony Brook. His research interests include development and clinical applications of innovative x-ray imaging modalities.

Brandon Nelson is a second-year graduate student at the Mayo Clinic Graduate School of Biomedical Sciences in the Department of Biomedical Engineering and Physiology. He received his BA degree in physics from Carleton College in 2016. His research interest is in advanced CT technology.

Shuai Leng received his BS degree in engineering physics in 2001, an MS degree in engineering physics in 2003, from Tsinghua University, and a PhD in medical physics in 2008 from the University of Wisconsin, Madison, USA. He is an associate professor of medical physics at the Mayo Clinic in Rochester, Minnesota, USA. He has authored over 100 peer-reviewed articles. His research interest is technical development and clinical application of x-ray and CT imaging.

Cynthia H. McCollough is a professor of radiological physics and biomedical engineering at Mayo Clinic, where she directs the CT Clinical Innovation Center. Her research interests include CT dosimetry, advanced CT technology, and new clinical applications, such as dual-energy and multispectral CT. She is an NIH-funded investigator and is active in numerous professional organizations. She is a fellow of the AAPM and ACR. She received her doctorate from the University of Wisconsin in 1991.

William S. Graves is an associate professor of physics and the Biodesign Institute at Arizona State University. He is a director of ASU's Compact X-Ray Light Source project designed to bring synchrotron-like x-ray beams into small labs. His interests are in the physics of coherent x-ray generation and generation of bright electron beams for a wide range of applications. He received his doctorate from the University of Wisconsin-Madison in 1994.